

Importance of Bone Attenuation in Brain SPECT Quantification

Robert Z. Stodilka, Brad J. Kemp, Frank S. Prato and Richard L. Nicholson

Department of Nuclear Medicine and Magnetic Resonance, St. Joseph's Health Centre, Lawson Research Institute, and Department of Medical Biophysics, University of Western Ontario, London, Ontario, Canada

The purpose of this study was to determine the effects of nonuniform attenuation on relative quantification in brain SPECT and to compare the ability of the Chang and Sorenson uniform attenuation corrections (UACs) to achieve volumetric relative quantification. **Methods:** Three head phantoms (dry human skull, Rando and Radiology Support Devices (RSD) phantoms) were compared with a human head using a gamma camera transmission CT (γ TCT) SPECT system and x-ray CT. Subsequently, the RSD phantom's brain reservoir was filled with a uniform water solution of ^{99m}Tc , and SPECT and γ TCT data were acquired using fanbeam collimation. The attenuating effects of bone, scalp and head-holder in individual projections were determined by an analytical projection technique using the SPECT and γ TCT reconstructions. The Chang UAC used brain and head contours that were segmented from the γ TCT reconstruction to demarcate its attenuation map, whereas the Sorenson UAC fit slice-specific ellipses to the SPECT projection data. For each UAC, volumetric relative quantification was measured with varying attenuation coefficients (μ s) of the attenuation map. **Results:** Gamma camera transmission CT and x-ray CT scans showed that the dry skull and Rando phantoms suffered from a dried trabecular bone compartment. The RSD phantom most closely reproduced the attenuation coefficients of the human γ TCT and x-ray CT scans. The analytical projections showed that the attenuating effects of bone, scalp and head-holder were nonuniform across the projections and accounted for 18%–37% of the total count loss. Volumetric relative quantification was best achieved with the Chang (zero iterations) attenuation correction using the head contour and $\mu = 0.075 \text{ cm}^{-1}$; however, cortical activity was found to be 10% higher than cerebellar activity. For all UACs, the optimal choices of μ were experimentally found to be lower than the recommended 0.12 cm^{-1} for brain tissue. This result is theoretically supported here. **Conclusion:** The magnitude of errors resulting from uniform attenuation corrections can be greater than the magnitudes of regional cerebral blood flow deficits in patients with dementia, as compared with normal controls. This suggests that nonuniform attenuation correction in brain SPECT imaging must be applied to accurately estimate regional cerebral blood flow.

Key Words: brain SPECT attenuation; head phantom; Chang attenuation correction; Sorenson attenuation correction

J Nucl Med 1998; 39:190–197

Regional cerebral blood flow has been measured using SPECT to aid in diagnosing dementias, such as Alzheimer's disease (1,2). Conventional filtered backprojection, however, provides reconstructions that are not relatively quantitative, that is, the counts-to-pixel ratios from two different regions do not accurately represent the ratio of radioactivity in the corresponding anatomical locations. The major hindrance to quantification is attenuation, or the absorption of gamma rays. Attenuation reduces lesion contrast, producing "hot-rim" artifacts (3), and

generally results in an underestimation of radiopharmaceutical concentration.

Many attenuation correction methods exist (4–7), each making different assumptions regarding the distribution of radioactivity or attenuation properties of the medium in which the radiopharmaceutical is present. Notwithstanding the conditions of brain SPECT, in which the radiopharmaceutical is distributed within a homogeneous medium (the brain) that is completely surrounded by an outer medium of different composition (the skull), it remains debatable as to whether this outer medium needs to be considered when correcting for attenuation. Turkington et al. (8) have shown that the attenuating effects of a dry skull are negligible and suggest that a uniform attenuation correction (UAC) is sufficient. Investigators, using experiments (9), simulations (10,11) and clinical trials (12), have found, however, that attenuating effects due to bone make peripheral quantification difficult, particularly adjacent to regions of thick bone.

This work experimentally measured the effects of attenuation in brain SPECT using an anthropomorphic phantom and determined the accuracy with which a UAC can achieve volumetric relative quantification. This study was done in three parts. Several head phantoms were compared to in vivo human scans using two imaging modalities: gamma camera transmission CT (13) (γ TCT) and x-ray CT. After selection of the phantom that best represented the in vivo conditions, attenuating effects in individual projections were determined by an analytical projection technique. The Chang (4) and Sorenson (5) UACs were then compared because they are in wide clinical use by companies such as General Electric, Siemens, Picker, Elscint and ADAC. Finally, in the Appendix, we show that the optimal attenuation coefficient used in UAC for brain SPECT is highly dependent upon skull thickness.

MATERIALS AND METHODS

Experiments

Three different phantoms were evaluated in this study: a dry human skull, the nine superior slices of a Rando phantom (Alderson Research Laboratories, Long Beach, CA) and a Radiology Support Devices (RSD) prototype head phantom (Radiology Support Devices, Inc., Long Beach, CA). The Rando phantom is an axially-sectioned human skull, embedded within synthetic isocyanate rubber (14), that mimics the attenuation effects of soft tissue and is designed for dosimetry measurements. The RSD head phantom is an artificial skull enclosed within material that mimics soft tissue, including ears, nose and neck. In this study, a removable single-compartment brain reservoir was used. A small air space was noticed between the skull enclosure and brain reservoir; this was filled with water-equivalent gelatin.

The attenuation coefficient distributions of the human skull, Rando and RSD phantoms were measured using x-ray CT and γ TCT. The phantoms were imaged with x-ray CT (High Speed Advantage RP; General Electric, Milwaukee, WI) at 120 kVp and

Received Sep. 4, 1996; revision accepted Mar. 25, 1997.
For correspondence or reprints contact: Frank S. Prato, PhD, Department of Nuclear Medicine, St. Joseph's Health Centre, 268 Grosvenor Street, London, Ontario, Canada, N6A 4V2.

reconstructed into 512×512 axial tomographs, each being 3 mm thick and having a 250-mm field of view (FOV). The γ TCT system has been previously described in detail (13). It consists of a SPECT system (Starcam 400AC; General Electric, Milwaukee, WI) with a fanbeam collimator (Nuclear Fields, Des Plaines, IL), having a 600-mm focal length and 1.5-mm flat-to-flat hexagonal hole width. A frame was mounted onto the collimator that held a collimated ^{99m}Tc line source along the focal line of the collimator. The collimation of both the line source and detector minimizes scatter; hence, the system measures narrow-beam attenuation coefficients. A 128-projection dataset, equally spaced over 360° , was acquired with a 160-mm radius of rotation. Each projection was 128×128 pixels and had a 409.6-mm FOV. An energy window of 20%, centered on the ^{99m}Tc photopeak of 140 keV, was used. The scan was reconstructed into the object plane, which had a 265-mm FOV and 2.1-mm^2 pixels. All transmission projections were corrected using decay, energy, uniformity and linearity correction files. Projections were prefiltered with a Hann filter, with a cutoff frequency of 1.56 cm^{-1} , and reconstructed by filtered backprojection.

The in vivo human x-ray CT scan was acquired with the same parameters indicated above. Gamma camera transmission CT scanning time, however, was shortened when only 64 projections, each being 40 sec long, were acquired. These parameters are typical of a clinical scan.

To evaluate the narrow-beam attenuating effects in individual projections, registered SPECT and γ TCT images of the RSD phantom were first obtained. The RSD phantom was the phantom of choice among those listed because it most closely approximated the in vivo attenuation coefficient distribution. The RSD phantom was filled with a uniform solution of 450 MBq ^{99m}Tc in water, and a SPECT scan was acquired. The time per projection was 25 sec, allowing approximately 500,000 counts in the first projection. Before the γ TCT acquisition, the ^{99m}Tc solution within the phantom was allowed to decay over a period of 58 hr. The γ TCT scan was then obtained using the parameters indicated above. The phantom's position remained fixed throughout; thus, both SPECT and γ TCT datasets were registered.

Analysis

The phantoms were evaluated by comparing the profiles, taken through γ TCT and x-ray CT transverse images, with those of the in vivo human scans. Comparison was based on quantitative values of bone narrow-beam attenuation coefficients.

The narrow-beam attenuation effects of the RSD phantom were evaluated by analytically projecting the transverse SPECT-reconstructed images and incorporating attenuation by using the registered γ TCT-reconstructed images. Although the RSD phantom's brain reservoir contained a uniform distribution, the raw SPECT reconstruction was affected by attenuation and, consequently, had a lower count density in its central regions. Therefore, for this investigation, the reconstructed SPECT scan was forced to have a uniform count density throughout the brain: for a given slice, pixels with intensities greater than 30% of the maximum intensity were set to unity, and those equal to or below the 30% threshold were set to zero. The bone, scalp and head-holder (BSH) were segmented from the original γ TCT image ($\text{Tx}_{\text{BR}+\text{BSH}}$) using a software package (15) to produce a γ TCT image containing brain tissue only (Tx_{BR}). Lateral and posterior analytical projections were produced at the cortical and cerebellar levels using both Tx_{BR} and $\text{Tx}_{\text{BR}+\text{BSH}}$. The nonuniform effects due to BSH were evaluated by dividing the projections attenuated with Tx_{BR} (Proj_{BR}) by the corresponding projections attenuated with $\text{Tx}_{\text{BR}+\text{BSH}}$ ($\text{Proj}_{\text{BR}+\text{BSH}}$). The percentage of count loss due to BSH was estimated to be:

$$\left[1 - \left(\frac{\sum_{\text{projection}} \text{Proj} - \sum_{\text{projection}} \text{Proj}_{\text{BR}}}{\sum_{\text{projection}} \text{Proj} - \sum_{\text{projection}} \text{Proj}_{\text{BR}+\text{BSH}}} \right) \right] \times 100\%, \text{ Eq. 1}$$

where Proj is the unattenuated projection, and the sums are taken over all pixels in the corresponding projections.

Three UACs were evaluated: the multiplicative Chang (4) (Chang0), one iteration of the iterative Chang (Chang1) and the Sorenson (5). Chang0 is a prereconstruction UAC that is analytically exact for a point source of activity, whereas Chang1 is an iterative modification that attempts to correct a reconstruction if multiple or distributed sources are present. The Sorenson prereconstruction UAC is an exact solution for a uniform distribution of radioactivity.

Each UAC requires the demarcation of object contours to define the attenuation map. The Chang UACs were performed using both brain contour and head contour (BC and HC, respectively), which were segmented from reconstructed γ TCT data, whereas the Sorenson method used slice-specific ellipses that were fit to the SPECT projection data.

The attenuation maps also require the assignment of an attenuation coefficient (μ). Uniform attenuation correction in brain imaging commonly uses $\mu = 0.12\text{ cm}^{-1}$; this value corresponds to the broad-beam attenuation coefficient of water, with a 20% energy acquisition window. There has been debate indicating that this may not be a suitable choice for μ in brain imaging (9,16); therefore, reconstructions were performed for each UAC using several values of μ , as follows: 0, 0.03, 0.05, 0.07, 0.075, 0.09, 0.12, 0.15 and 0.19 cm^{-1} . Based on three relative quantification metrics that are described below, optimal values of μ were selected for each UAC and contour.

Although the SPECT volume is corrected with a single μ for each reconstruction, the UACs treat slices as independent. There is, however, considerable axial variation in the head. Consequently, by correcting a volumetric dataset with a μ optimized for one particular slice, reconstructed count densities in other slices may be undesirably affected. This effect was measured in three ways:

1. In the first method, the coefficient of variation (CoV) of activity among 450 uniformly spaced cubic regions of interest (ROIs) was plotted as a function of μ for each UAC. This metric would identify the μ that provided the best overall volumetric relative quantification for each UAC.
2. In the second method, two ROIs were defined in a cortical slice, then normalized to a ROI in a cerebellar slice and plotted as a function of μ . Cerebellar normalization is commonly done in studies dealing with Alzheimer's disease (2) and receptor imaging (17). This analysis indicates how optimizing a UAC, for the purpose of improving the accuracy of relative quantification in one slice, will affect the accuracy of volumetric relative quantification.
3. Finally, 5-pixel-thick profiles were selected in cortical and cerebellar slices, and the count density as a function of position in each profile was fit by least squares to a parabolic equation of the form: $\text{count-density}(\text{pixel}) = C_2(\text{pixel})^2 + C_0$. C_2 measures a UAC's ability to reconstruct uniform profiles, which is indicated by $C_2 = 0$. A C_2 greater than zero indicates that the count density in the central region of the head is lower than that near the periphery. Conversely, when C_2 is less than zero, the periphery has a higher count density than the center. A plot of C_2 against μ was constructed to find the optimal μ for a given slice, defined as that which yields a uniform profile.

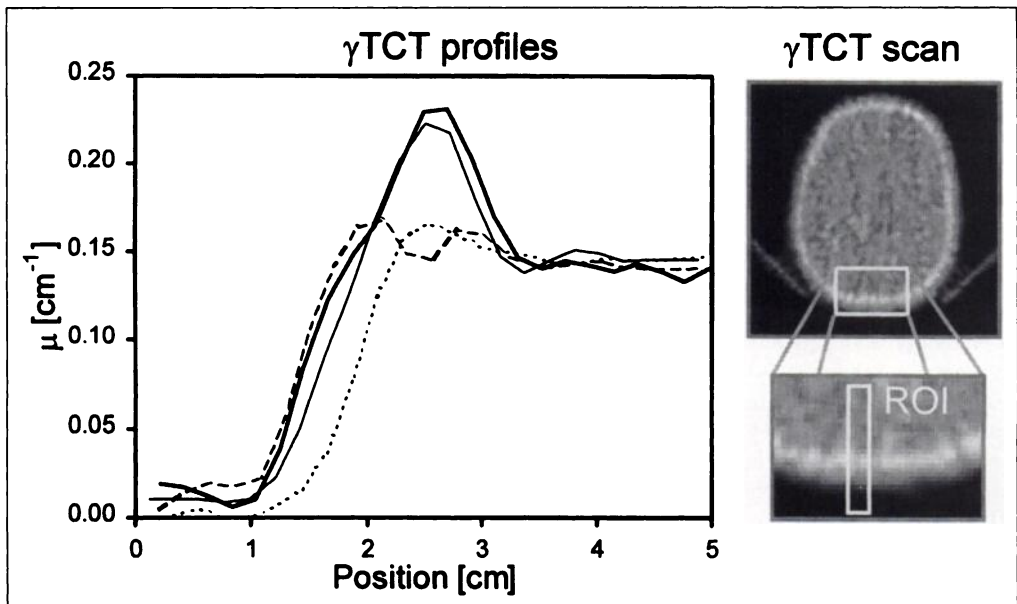


FIGURE 1. Gamma camera transmission CT head phantom comparison at the cortical level. Profiles of three phantoms (···, skull; ---, Rando; —, RSD) were compared with that of a human (—). Both the Rando and skull showed reduced attenuation coefficients of the skull due to a deteriorated trabecular bone compartment. The sample image is that of the human and shows the location of the ROI from which the profile was taken.

This last metric was used to indicate how selection of an optimal μ varies between slices, as well as to confirm the results from the second metric described above.

RESULTS

Phantom Selection

Gamma camera transmission CT scan profiles for each phantom are compared with in vivo human scans in Figure 1. The profiles were taken at the cortical level, beginning posterior and extending through the skull and into the brain. The bone attenuation coefficients for the RSD phantom were found to be closest to the in vivo scans. The bone attenuation coefficients of both the skull and Rando phantoms were found to be significantly lower. The higher resolution of the x-ray CT scans (Fig. 2) revealed that this was due to deterioration of the trabecular bone compartment. In vivo trabecular bone is composed of a compact bone matrix and fat- or liquid-filled interstices. The skull and Rando phantoms, however, had dried significantly.

Attenuation in Projections

Registered SPECT and γ TCT ($T_{X_{BR+BSh}}$) scans from a cortical slice are shown in Figure 3A and B, respectively. Figure 3C shows posterior Proj, Proj_{BR} and Proj_{BR+BSh} pro-

files. Bone, scalp and head-holder were found to account for an average of 18% of the total count loss due to attenuation in this projection; BSH attenuation effects are summarized in Table 1. Figure 3D demonstrates how Proj_{BR}/Proj_{BR+BSh} varies with position, indicating the effect of BSH to be greater at the periphery of the projection, where gamma rays must traverse the skull obliquely. The BSH effect was found to be greatest for lateral projections at the cerebellar level, where BSH accounted for 38% of the total counts lost due to attenuation.

Evaluation of Uniform Attenuation Corrections

Figure 4 indicates the BC and HC for cortical and cerebellar slices. As indicated above, these contours were used for both Chang0 and Chang1.

The volumetric CoV, as a function of μ , has one global minimum for each UAC. These minima, as well the variation of CoV with μ for Chang0-HC, are shown in Figure 5A. Chang0-HC, with $\mu = 0.075 \text{ cm}^{-1}$, was found to be the best overall UAC because it produced the smallest volumetric CoV, which was 4.1%. The CoV of the data was statistically limited to approximately 1%.

The two cortical ROIs, represented in Figure 6B as alpha and beta, were normalized to the cerebellar ROI, represented as

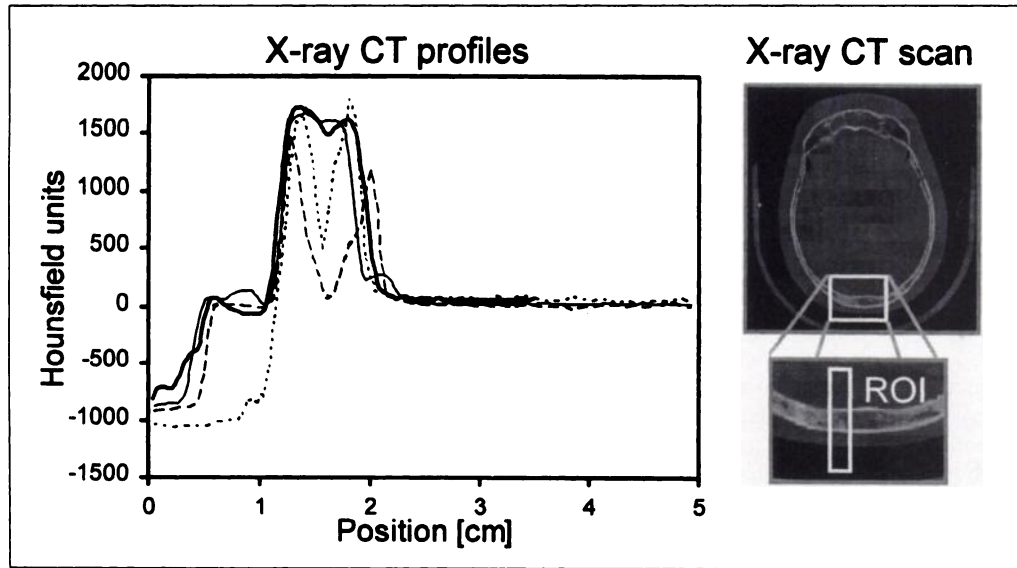


FIGURE 2. X-ray CT head phantom comparison at the cortical level. Profiles of three phantoms (···, skull; ---, Rando; —, RSD) were compared with that of a human (—) on the plot. The sample image is of the Rando phantom and shows the location of the ROI from which the profile was taken. This also shows the significant trabecular bone compartment deterioration of the Rando and skull phantoms and the lack of scalp on the skull phantom.

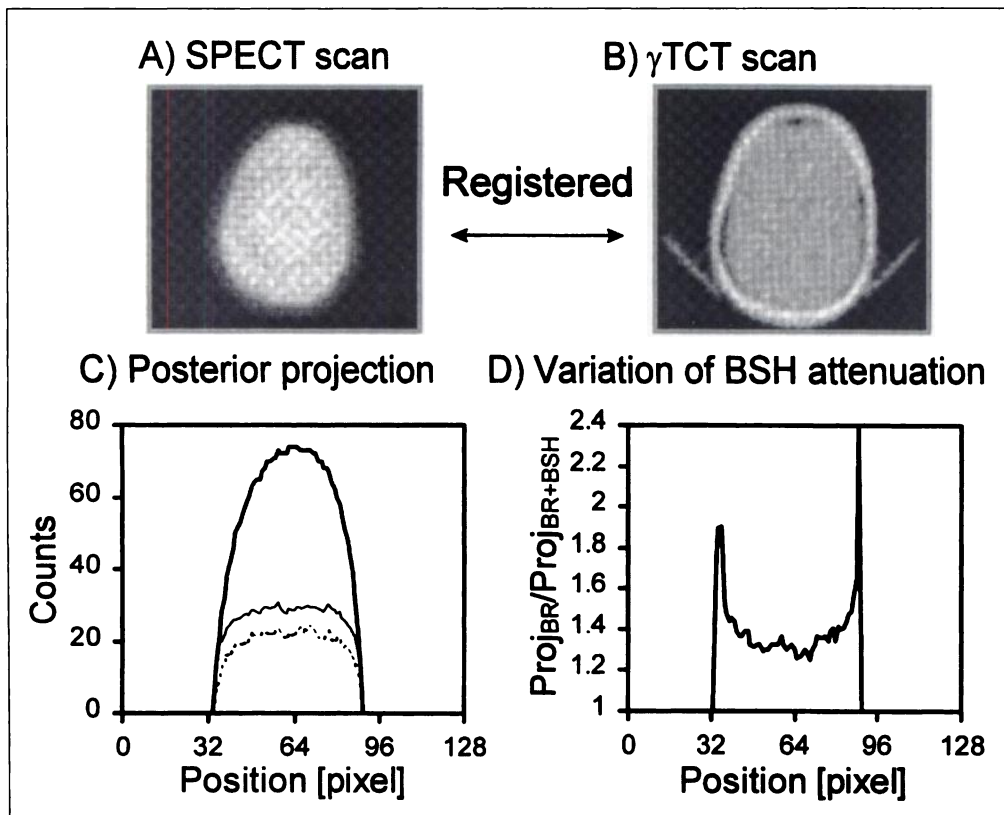


FIGURE 3. Registered (A) SPECT and (B) γ TCT images of the RSD phantom were used to produce analytical projections to investigate the effects of narrow-beam attenuation. (C) Posterior unattenuated projection of image in A, Proj (—); attenuation only due to brain tissue, Proj_{BR} (---); and attenuation by both brain and BSH, Proj_{BR+BSH} (····). (D) Spatial variance of Proj_{BR}/Proj_{BR+BSH}.

gamma, in Figure 6C. For each UAC, relative quantification is achieved within the cortical slice when the alpha/gamma and beta/gamma intersect, at some μ . This intersection also indicates the reconstructed activity of the cortical slice, relative to the cerebellar slice. Cortical activity, relative to cerebellar, was most accurately achieved, again, by Chang0-HC, but with $\mu = 0.087 \text{ cm}^{-1}$. In this case, the error in relative quantification was 9.5%.

Table 2 indicates the value of μ that produced the flattest profiles, as measured by the parabolic equation, for each UAC in cortical and cerebellar slices. Example profiles for Chang0-HC and Sorenson are shown in Figure 7. In all cases, the optimal selection of μ was less than the brain tissue attenuation coefficient of $\mu = 0.12 \text{ cm}^{-1}$. Note that, for all UACs, the optimal μ for the cerebellar slice was lower than that for a cortical slice.

DISCUSSION

Phantom Selection

Trabecular bone is a composite material consisting of a matrix of compact bone and water- or fat-filled interstices. Both natural phantoms, the skull and the Rando, had significantly

dried in their curing process; hence, their interstices contained only air. It should be emphasized that, because the γ TCT is unable to resolve in vivo compact bone from trabecular bone, γ TCT skull attenuation coefficients never reach those of compact bone, which is 0.28 cm^{-1} at 140 keV (18,19).

The RSD phantom was found to be the most suitable for investigating the attenuation effects of brain SPECT. The significant trabecular deterioration of the skull and Rando phantoms suggests that previous attenuation and scatter measurements using skull phantoms (8) have underestimated both the magnitude and characteristics of skull effects.

Air spaces in the RSD phantom γ TCT scan were noticed between the skull enclosure and brain reservoir, despite significant effort to completely fill them with gelatin. These spaces can be seen in the lateral and frontal regions of Figure 3B. A

TABLE 1
Effects of Attenuation on Individual Projections*

Projection	Cortical		Cerebellar		CoV (%)
	Posterior	Lateral	Posterior	Lateral	
RSD (% total count loss)	66.6	58.2	60.8	65.3	6
RSD (% BSH count loss)	18.4	21.3	31.3	37.6	33

*Attenuating effects were measured by comparing unattenuated projections (Proj) with attenuated projections (Proj_{BR} and Proj_{BR+BSH}). Attenuation due to the combined brain and BSH was greatest for cortical posterior and cerebellar lateral projections; however, attenuation due to BSH was found to be markedly greater for cerebellar lateral than cortical posterior projections.

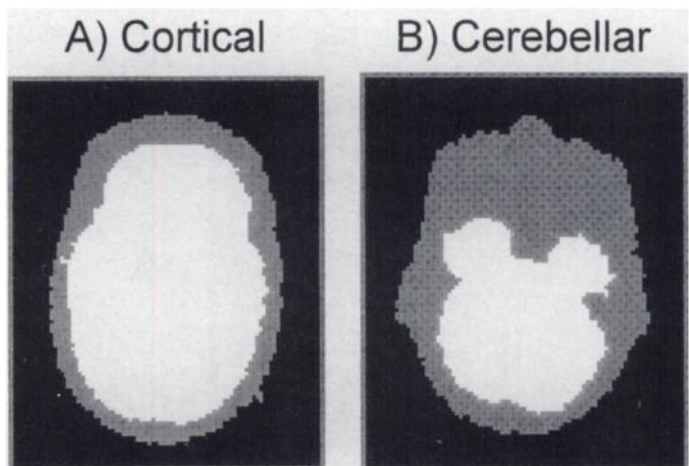


FIGURE 4. Brain contour (white) and head contour, segmented from a γ TCT scan. These contours defined the uniform attenuation maps used in the Chang0 and Chang1 UACs. Note the considerable difference in the contours for the cerebellar slice.

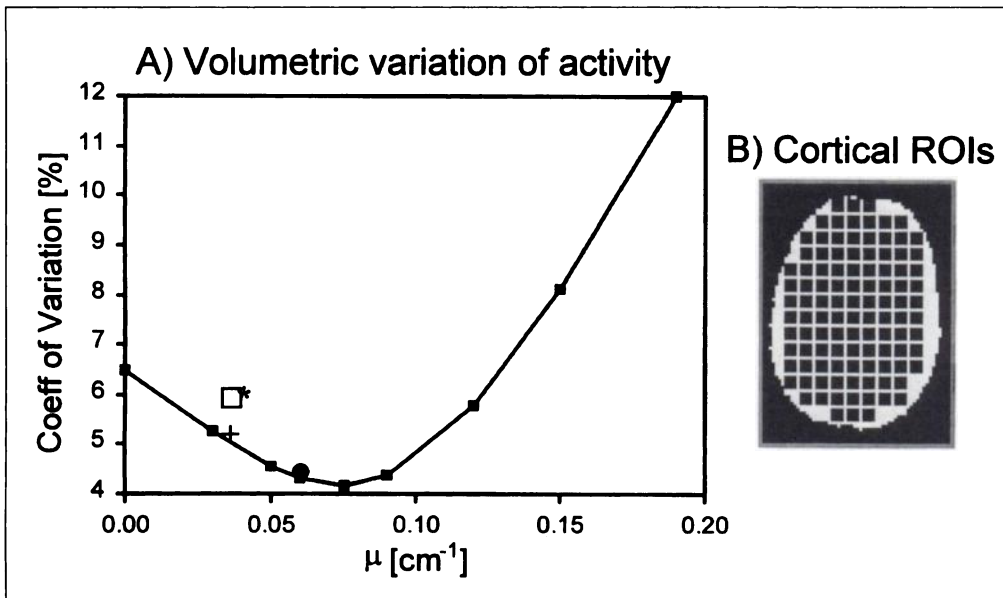


FIGURE 5. (A) Volumetric relative quantification was measured by the CoV metric. This variation, as a function of μ , is plotted for Chang0-HC (■), which was found to be the best UAC. Also indicated are the CoV minima for Chang0-BC (□), Chang1-BC (*), Chang1-HC (●) and Sorenson (+). (B) Cortical slice that indicates a subset of the ROIs from which the CoV was calculated.

small air gap may also exist at the back of the phantom. This may have contributed, as a partial volume effect, to the slight discrepancy in the skull attenuation coefficients of the human and RSD phantom, as can be seen in Figure 1.

Attenuation in Projections

The CoV of the percentage BSH count loss in Table 1 is significantly more than that of percentage total count loss. This indicates that, although the fluctuation of total count loss remains relatively small, the attenuation caused by BSH is highly nonuniform.

The issue of scatter was not addressed. SPECT scans have only detector collimation and contain scattered photons. Consequently, they are subject to broad-beam attenuation. The γ TCT scans, however, have the benefit of simultaneous source and detector collimation, which largely eliminates scatter in the γ TCT scans; they are a measure of narrow-beam attenuation coefficients (13). Strictly speaking, then, because the SPECT and γ TCT data were acquired under different conditions, the γ TCT data cannot be properly used to measure attenuation in SPECT projections without modifying the narrow-beam attenuation coefficients to broad-beam coefficients. Broad-beam

attenuation coefficients are, however, geometry-dependent. They are anisotropic and vary with projection angle, and so, no tomographic technique for measuring them has been devised.

Evaluation of Uniform Attenuation Correction

The plot of the normalized activity against μ (Fig. 6A) has three important characteristics that are common to each UAC:

1. The normalized activity of the inner ROI, beta, increases with μ , whereas the outer ROI, alpha, decreases.
2. The normalized activities for ROIs alpha and beta intersect at values of μ lower than 0.12 cm^{-1} . These results are consistent with the parabolic fit analysis, discussed below.
3. The normalized ROI activities do not intersect at a relative activity of one, indicating that the UACs cannot achieve volumetric relative quantification. In fact, each intersection is always greater than unity; cerebellar activity is always underestimated with respect to cortical activity.

As indicated in Table 2, for ideal relative quantification, a smaller value of μ was needed to correct for attenuation in a cerebellar slice than in a cortical slice. This result is contrary to previous speculation (16) and is counterintuitive because the

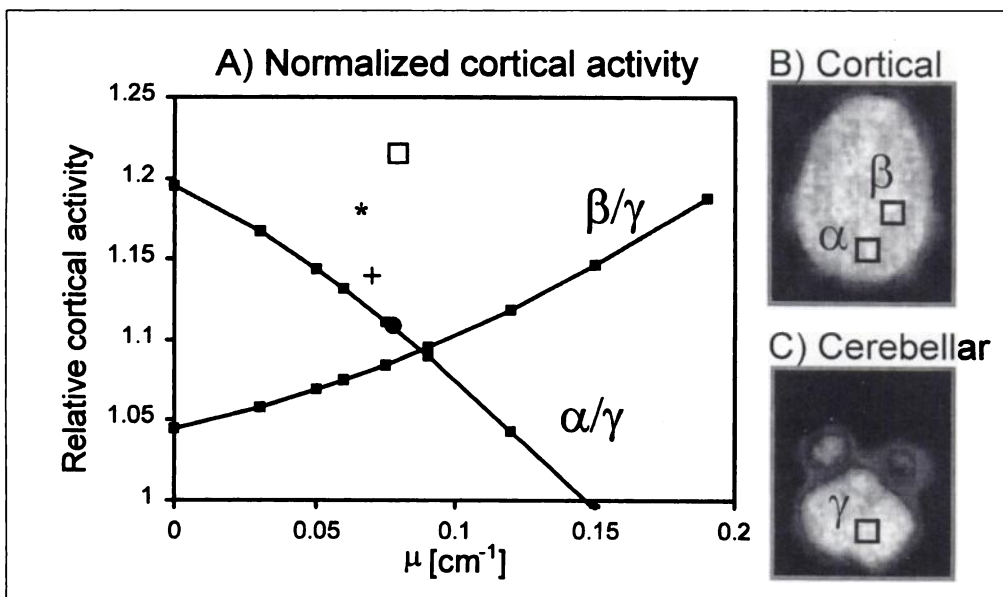


FIGURE 6. (A) Investigation of the effect of UAC on relative quantification. (B,C) Cortical and cerebellar images, respectively, of the RSD phantom filled with a uniform solution of ^{99m}Tc in water. The two cortical ROIs (α and β in B) were normalized to a cerebellar ROI (γ in C). The normalized activities show how the choice of μ affects the accuracy of volumetric relative quantification. This variation is plotted for Chang0-HC (■), which was found to be best. Also shown are the intersection points for Chang0-BC (□), Chang1-BC (*), Chang1-HC (●) and Sorenson (+).

TABLE 2
Selection of Optimal μ Based on a Parabolic Equation

UAC*	Contour	Optimal μ (cm^{-1})	
		Cortical	Cerebellar
Chang0	BC	0.081	0.062
Chang0	HC	0.089	0.078
Chang1	BC	0.061	0.049
Chang1	HC	0.077	0.067
Sorenson	BC	0.034	0.021

*For each UAC, optimal μ s were lower than the soft tissue μ of 0.12 cm^{-1} . In addition, μ s optimized for cerebellar slices always were lower than μ s optimized for cortical slices.

cerebellar slice is surrounded by thicker bone structures than is the cortical slice. This effect of thick bone on UAC effect was first noticed by Nicholson et al. (20) and was later experimentally demonstrated by Kemp et al. (9). It also can be theoretically shown for a disk of uniformly attenuating material, containing a uniform distribution of radioactivity, that the μ required to best correct for attenuation *decreases* as outer layers of attenuating material, free of radioactivity, are added. The Appendix shows that this applies to both the Chang0 and Sorenson UACs. This result is consistent with the findings of Kemp et al. (9), who indicate that a μ of 0.09 cm^{-1} produced the best attenuation correction when a dry human skull phantom containing a uniform solution of radioactivity is imaged. Furthermore, the theory predicts that the optimal μ for the RSD phantom should be lower than that for the dry skull because the x-ray CT profiles in Figure 2 indicate that the RSD phantom possesses a scalp, whereas the dry skull phantom does not. Additionally, as mentioned earlier, our findings indicate that the bone attenuation coefficients of the dry skull phantom are considerably less than those found in the RSD phantom and in vivo. This explains why our cortical optimal μ of 0.069 cm^{-1} for the Sorenson-corrected profile from the RSD phantom was lower than what was previously reported for the dry skull phantom.

The data presented indicates that using a μ of 0.12 cm^{-1} , as is common practice, results in an overestimated relative count density in the central regions of the brain, as compared with peripheral regions. The magnitude of the resulting error depends on the UAC and object contours used. In some cases,

however, the error can be larger than the measured regional cerebral blood flow deficits from patients with dementia, which is approximately 10% (2). More importantly, it has been shown that the optimal μ is slice-dependent, due to variations in the axial geometry of the head. Uniform attenuation correction cannot, therefore, simultaneously achieve relative quantification in more than one transaxial slice, unless the optimal μ is identical for the slices in question. This clearly presents a problem when relative counts from ROIs are measured across multiple slices (1,17) or volume data are resliced to extract anatomically important planes (2,21).

CONCLUSION

The errors in relative quantification caused by an attenuation correction that assumes the head to be a uniformly attenuating medium were found to be up to 20%, which is larger than regional cerebral blood flow deficits often reported in patients with dementia. Thus, the use of these attenuation corrections limits the accuracy of relative quantification and confounds the correlation between diagnosing dementia using brain SPECT compared to diagnosis by neuropsychological tests, such as the Dementia Rating Scale (22).

Clinically, many nonuniform attenuation corrections are used for SPECT scans involving organs found in the torso. Considering that quantification in brain SPECT is gaining importance in receptor imaging and diagnosing dementia, it is important that these techniques be extended to include the head.

ACKNOWLEDGMENTS

This research was supported in part by a university industrial grant from the Medical Research Council of Canada and General Electric Canada Grant UI-11814. We thank J. Van Dyk for the use of the Rando phantom and Dr. M. Basic and Radiology Support Devices, Inc., for their prototype striatal phantom. We also thank Dr. Peter Msaki for his advice and Aleks Cenic for acquiring the x-ray CT data.

APPENDIX

Mathematical Model

Improved single-slice relative quantification in brain SPECT relies on properly selecting the attenuation coefficient that is used in the Chang and Sorenson uniform attenuation corrections. The purpose of this Appendix is to show that the optimal selection of

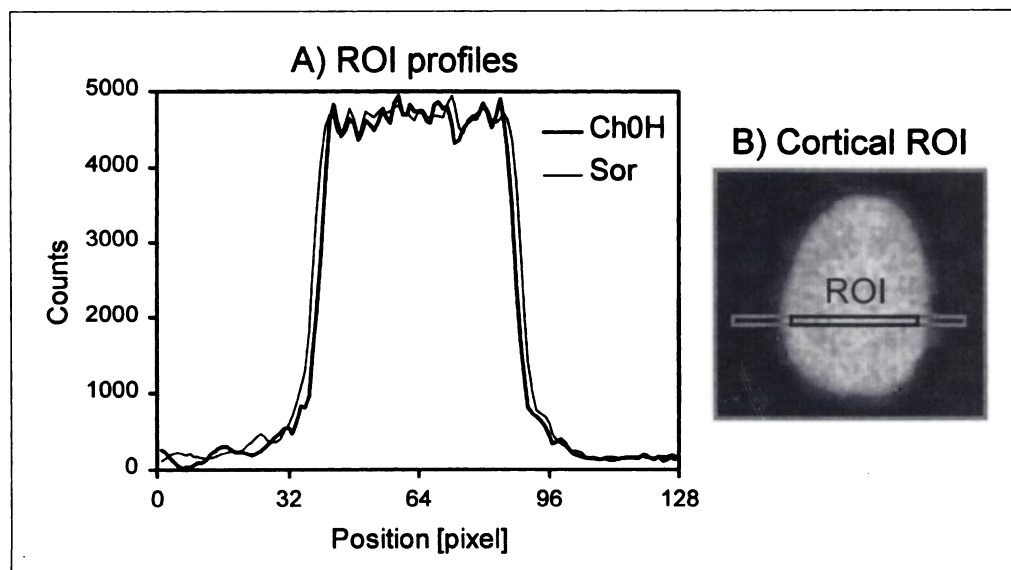


FIGURE 7. (A) Sample profiles taken from a ROI in a cortical slice (gray ROI in B). The profiles indicate the attenuation correction achieved by Chang0-HC with $\mu = 0.089 \text{ cm}^{-1}$ (—) and Sorenson with $\mu = 0.034 \text{ cm}^{-1}$ (---). These values of μ were optimized for this cortical slice by fitting parabolas to the black ROI in B.

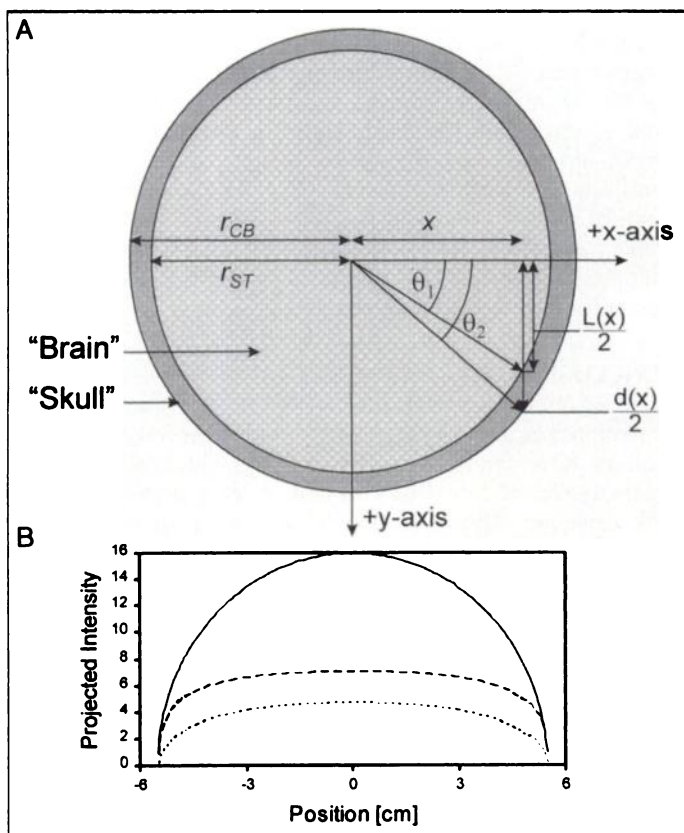


FIGURE 1a. (A) Mathematical head phantom in which the brain contains a uniform distribution of activity. (B) Projection without attenuation, Proj (—); attenuated by brain tissue, Proj_{ST} (---); and attenuated by brain and skull, Proj_{ST+CB} (···).

this attenuation coefficient is considerably dependent upon skull thickness.

The mathematical phantom presented assumes that the shape of the head can be approximated by a circle. Consider first the “brain”: a circle ST with radius r_{ST} , horizontally centered at $x = 0$ and filled with a uniform concentration of radioactivity of C (in Bq/cm^3), as indicated in Figure 1a. Defining θ_1 to be a function of horizontal position, x , as:

$$\theta_1(x) = \cos^{-1} \left(\frac{x}{r_{ST}} \right), \quad \text{Eq. 1a}$$

allows ST’s unattenuated projection (in the $+y$ direction in Fig. 8A) to be expressed as:

$$P(x) = 2 \cdot r_{ST} \cdot C \cdot \sin [\theta_1(x)]. \quad \text{Eq. 2a}$$

We also write the vertical pathlength through ST as a function of horizontal position to be:

$$L(x) = 2 \cdot r_{ST} \cdot \sin [\theta_1(x)]. \quad \text{Eq. 3a}$$

Note that for all equations, $|x| \leq r_{ST}$. Given that ST is characterized by an attenuation coefficient μ_{ST} , the attenuated projection is:

$$P_{ST}(x) = \int_{-(L(x)/2)}^{+(L(x)/2)} C \cdot \exp \left(- \int_y^{+(L(x)/2)} \mu_{ST} d\xi \right) dy. \quad \text{Eq. 4a}$$

A “skull” can be added to the phantom by surrounding ST with a concentric annulus, CB, representing cortical bone, with inner radius r_{ST} and outer radius r_{CB} . Noting that the angle θ_2 can be written as:

$$\theta_2(x) = \cos^{-1} \left(\frac{x}{r_{CB}} \right) \quad \text{Eq. 5a}$$

allows the vertical pathlength between two points on the outer perimeter of the annulus that are on opposite sides of the x -axis to be expressed as:

$$d(x) = 2 \cdot r_{CB} \cdot \sin [\theta_2(x)]. \quad \text{Eq. 6a}$$

The resulting attenuated projection of the activity can now be written in terms of $P_{ST}(x)$, $d(x)$ and the attenuation coefficient of the annulus, μ_{CB} :

$$P_{ST+CB}(x) = \exp \left(- \int_{(L(x)/2)}^{(d(x)/2)} \mu_{CB} d\xi \right) \cdot P_{ST}(x). \quad \text{Eq. 7a}$$

This equation approximates an acquired projection of a brain SPECT scan. The emitted signal from a distribution of radiopharmaceutical (uniform in this case) is attenuated both by the homogeneous medium within which it is contained and, subsequently, by a homogeneous medium that is external to the radiopharmaceutical distribution.

The prereconstruction Sorenson UAC applies a multiplicative term to modify $P_{ST+CB}(x)$ (5). The corrected attenuated projection, given μ , is:

$$SP_{ST+CB}(x) = \frac{\mu \cdot L(x)}{1 - \exp [-\mu \cdot L(x)]} \cdot P_{ST+CB}(x). \quad \text{Eq. 8a}$$

We now address the issue of how to properly assign a value to μ . Both $P(x)$ and $SP_{ST+CB}(x)$ can be normalized to their peaks, ($NP(x)$ and $NSP_{ST+CB}(x)$, respectively) clearly occurring at $x = 0$, as follows:

$$NP(x) = \frac{P(x)}{P(0)} \quad \text{Eq. 9a}$$

and

$$NSP_{ST+CB}(x) = \frac{SP_{ST+CB}(x)}{SP_{ST+CB}(0)}. \quad \text{Eq. 10a}$$

In selecting μ , one would intuitively expect that attenuation may be best compensated for by minimizing the difference between $NP(x)$ and $NSP_{ST+CB}(x)$. This optimal μ , μ^{OPT} , is defined as that μ which minimizes the root mean-square (RMS) error between $NP(x)$ and $NSP_{ST+CB}(x)$:

$$\mu^{OPT} = \min_{\mu} \left(\left\{ \int_{-r_{ST}}^{r_{ST}} [NP(x) - NSP_{ST+CB}(x)]^2 dx \right\}^{1/2} \right). \quad \text{Eq. 11a}$$

The multiplicative Chang UAC (4) was evaluated using an RMS metric similar to Equation 11a; however, the integral is evaluated across the reconstructed object rather than a projection of the object. Because the Chang UAC is a postreconstruction algorithm, the derivation of its RMS metric is too lengthy for presentation in this Appendix.

Relating the variables to brain imaging, at the gamma-ray energy for ^{99m}Tc , which is 140 keV, $\mu_{ST} = 0.12 \text{ cm}^{-1}$ (23) and $\mu_{CB} = 0.28 \text{ cm}^{-1}$ (18,19). The effect of skull thickness was examined by varying skull thickness between 0 cm and 1 cm; thus, $5.5 \leq r_{CB} \leq 6.5 \text{ cm}$.

Results

Plotting μ^{OPT} for skull thicknesses of 0–1 cm, as shown in Figure 2a, shows several important characteristics:

1. $\mu^{OPT} = \mu_{ST}$ for the Sorenson UAC when skull thickness is 0 cm. This was expected because this UAC is analytically correct for a uniform source in a homogeneous object.

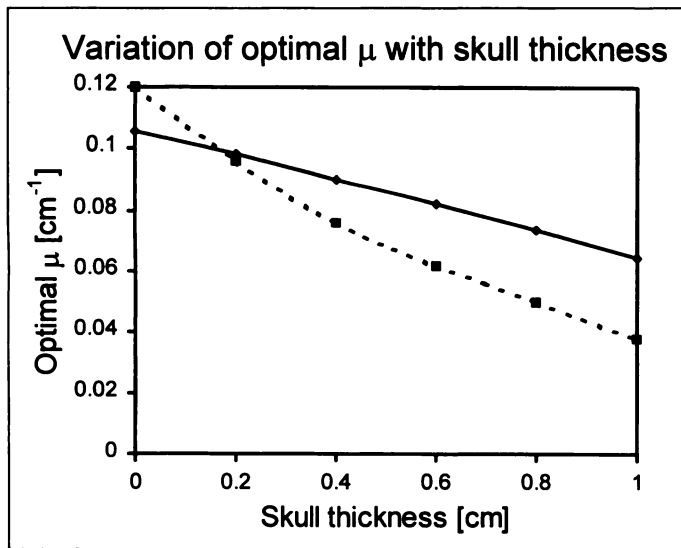


FIGURE 2a. Decrease of optimal μ as skull thickness increases. Curves shown are for Chang (—) and Sorenson (- - -) UACs.

- μ^{OPT} is a monotonically decreasing function for both the Chang and Sorenson UACs. Therefore, as the skull thickness increases, μ must decrease if optimal attenuation correction is to be maintained, not increase, as has been previously suggested (16).

It should be noted that the minimum RMS error (data not shown) equals zero only for the Sorenson UAC and a skull thickness of 0 cm (and increases almost linearly with CB thickness); thus, relative quantification within a slice can only be achieved by a UAC for a homogeneous medium.

Our method selects μ^{OPT} only by minimizing the RMS error between two *normalized* projections; a criterion for measuring how both skull thickness and the Sorenson and Chang UACs affect average count density has not been investigated. Clearly, Equation 7a indicates a reduction in count density as skull thickness increases, as is common in the cerebellar regions of the skull. The Chang and Sorenson UACs, however, increase the average count density as μ is increased. Because reducing μ is necessary to better correct for the nonuniform effects of attenuation within a slice with a thicker skull, improving relative quantification within that slice can only be done at the expense of reducing its average count density, as has been experimentally demonstrated (9). Furthermore, if skull thickness varies between slices, then this result indicates that volumetric relative quantification using UAC cannot be achieved. Kemp et al. (9) have proposed a modification to the Sorenson algorithm that separately compensates for the attenuating

effects of soft tissue and the skull; however, the spatial distribution of the skull must be known a priori.

REFERENCES

- Perani D, Di Piero V, Vallar G, et al. Technetium-99m-HMPAO-SPECT study of regional cerebral perfusion in early Alzheimer's disease. *J Nucl Med* 1988;29:1507-1514.
- Karbe H, Kertesz A, Davis J, Kemp BJ, Prato FS, Nicholson RL. Quantification of functional deficit in Alzheimer's disease using a computer-assisted mapping program for ^{99m}Tc-HMPAO SPECT. *Neuroradiology* 1994;36:1-6.
- Budinger TF, Gullberg GT, Huesman RH. Emission computed tomography. In: Herman GT, ed. *Image reconstruction from projections: implementation and applications*. New York: Springer-Verlag; 1979:147-246.
- Chang LT. A method for attenuation correction in radionuclide computed tomography. *IEEE Trans Nucl Sci* 1978;25:638-643.
- Sorenson JA. Quantitative measurement of radioactivity in vivo by whole body counting. In: Hine GJ, Sorenson JA, eds. *Instrumentation in nuclear medicine*. New York: Academic Press; 1974:311-348.
- Bellini S, Piacentini M, Cafforio C, Rocca F. Compensation of tissue absorption in emission tomography. *IEEE Trans Acoust Speech Signal Processing* 1979;27:213-218.
- Shepp LA, Vardi Y. Maximum likelihood reconstruction for emission tomography. *IEEE Trans Med Imaging* 1982;2:113-122.
- Turkington TG, Gilland DR, Jaszczak RJ, Greer KL, Coleman RE. A direct measurement of skull attenuation for quantitative SPECT. *IEEE Trans Nucl Sci* 1993;40:1158-1161.
- Kemp BJ, Prato FS, Dean GW, Nicholson RL, Reese L. Correction for attenuation in technetium-99m-HMPAO SPECT brain imaging. *J Nucl Med* 1992;33:1875-1880.
- Galt JR, Yin G, Cullom SJ, Halkar RK. Pitfalls and problems of conventional attenuation correction for brain SPECT [Abstract]. *Radiology* 1995;197:452P.
- Glick SJ, King MA, Pan TS, Soares EJ. Compensation for nonuniform attenuation in SPECT brain imaging. *IEEE Trans Nucl Sci* 1996;43:737-750.
- Zhang JJ, Park CH, Kim SM, Reyes P. Attenuation effect of brain SPECT [Abstract]. *J Nucl Med* 1992;33:961.
- Kemp BJ, Prato FS, Nicholson RL, Reese L. Transmission computed tomography imaging of the head with a SPECT system and a collimated line source. *J Nucl Med* 1995;36:328-335.
- White DR. Tissue substitutes in experimental radiation physics. *Med Phys* 1978;5:467-479.
- Robb RA. A software system for interactive and quantitative analysis of biomedical images. In: Hohne KH, Fuchs H, Pizer SM, eds. *3D imaging in medicine*, NATO ASI series 60, Vol. F. Berlin: Springer-Verlag; 1990:333-361.
- Croft BY. *Single-photon emission computed tomography*. New York: Year Book Medical Publishers; 1986:241.
- Chabriet H, Levasseur M, Vidailhet M, et al. In-vivo SPECT imaging of D2 receptor with iodine-iodolisuride: results in supranuclear palsy. *J Nucl Med* 1992;33:1481-1485.
- NIST. *X-ray and gamma ray attenuation coefficient and cross-section database*, Version 2.0. Gaithersburg, MD: U.S. Department of Commerce, National Institute of Standards and Technology, Standard Reference Data Program; 1988.
- White DR, Widdowson EM, Woodard HQ, Dickerson JWT. The composition of body tissues. *Br J Radiol* 1991;64:149-159.
- Nicholson RL, Doherty M, Wilkins K, Prato FS. Paradoxical effect of the skull on attenuation correction requirements for brain SPECT [Abstract]. *J Nucl Med* 1988;29:1316P.
- Johnson KA, Mueller ST, Walshe TM, English RJ, Holman BL. Cerebral perfusion imaging in Alzheimer's disease: use of single photon emission computed tomography and iofetamine hydrochloride I-123. *Arch Neurol* 1987;44:165-168.
- Mattis S. *DRS, dementia rating scale*, professional manual. Odessa, FL: Psychological Assessment Resources; 1988.
- Harris CC, Greer KL, Jaszczak RJ, Floyd CE, Fearnow EC, Coleman RE. Tc-99m attenuation coefficients in water-filled phantoms determined with gamma cameras. *Med Phys* 1984;11:681-685.